
Full-length Article

# Non-invasive PET imaging of brain inflammation at disease onset predicts spontaneous recurrent seizures and reflects comorbidities

Daniele Bertoglio, Jeroen Verhaeghe, Eva Santermans, Halima Amhaoul, Elisabeth Jonckers, Leonie Wyffels, Annemie Van Der Linden, Niel Hens, Steven Staelens, Stefanie Dedeurwaerdere

PII: S0889-1591(16)30563-3
DOI: http://dx.doi.org/10.1016/j.bbi.2016.12.015
Reference: YBRBI 3047

To appear in: *Brain, Behavior, and Immunity*

Received Date: 13 October 2016
Revised Date: 5 December 2016
Accepted Date: 18 December 2016

Please cite this article as: Bertoglio, D., Verhaeghe, J., Santermans, E., Amhaoul, H., Jonckers, E., Wyffels, L., Van Der Linden, A., Hens, N., Staelens, S., Dedeurwaerdere, S., Non-invasive PET imaging of brain inflammation at disease onset predicts spontaneous recurrent seizures and reflects comorbidities, *Brain, Behavior, and Immunity* (2016), doi: http://dx.doi.org/10.1016/j.bbi.2016.12.015

# Non-invasive PET imaging of brain inflammation at disease onset predicts spontaneous recurrent seizures and reflects comorbidities

Daniele Bertoglio[1], Jeroen Verhaeghe[2], Eva Santermans[3], Halima Amhaoul[1], Elisabeth Jonckers[4], Leonie Wyffels[2,5], Annemie Van Der Linden[4], Niel Hens[3,6], Steven Staelens[2], Stefanie Dedeurwaerdere[1]

[1]University of Antwerp, Department of Translational Neurosciences, Wilrijk, Belgium

[2]University of Antwerp, Molecular Imaging Center Antwerp, Wilrijk, Belgium

[3]Interuniversity Institute for Biostatistics and Statistical Bioinformatics, Hasselt University, Diepenbeek, Belgium

[4]University of Antwerp, Bio-Imaging Lab, Wilrijk, Belgium

[5]Antwerp University Hospital, Department of Nuclear Medicine, Edegem, Belgium

[6]Centre for Health Economics Research and Modelling Infectious Diseases, Vaccine and Infectious Disease Institute, University of Antwerp, Antwerp, Belgium

## Abstract

Brain inflammation is an important factor in the conversion of a healthy brain into an epileptic one, a phenomenon known as epileptogenesis, offering a new entry point for prognostic tools. The development of anti-epileptogenic therapies to treat before or at disease onset is hampered by our inability to predict the severity of the disease outcome. In a rat model of temporal lobe epilepsy we aimed to assess whether *in vivo* non-invasive imaging of brain inflammation at disease onset was predictive of spontaneous recurrent seizures (SRS) frequency and severity of depression-like and sensorimotor-related comorbidities. To this end, translocator protein, a biomarker of inflammation, was imaged by means of positron emission tomography (PET) 2 and 4 weeks post-status epilepticus using [$^{18}$F]-PBR111. Translocator protein was highly upregulated 2 weeks post-status epilepticus in limbic structures (up to 2.1-fold increase compared to controls in temporal lobe, $P < 0.001$), whereas 4 weeks post-status epilepticus, upregulation decreased (up to 1.6-fold increase compared to controls in temporal lobe, $P < 0.01$) and was only apparent in a subset of these regions. Animals were monitored with video-electroencephalography during all stages of disease (acute, latent – first seizures appearing around 2 weeks post-status epilepticus - and chronic phases), for a total of 12 weeks, in order to determine SRS frequency for each subject (range 0.00 – 0.83 SRS/day). We found that regional PET uptake at 2 and 4 weeks post-status epilepticus correlated with the severity of depression-like and sensorimotor-related comorbidities during chronic epilepsy ($P < 0.05$ for each test). Regional PET imaging did not correlate with SRS frequency, however, by applying a multivariate data-driven modeling approach based on translocator protein PET imaging at 2 weeks post-status epilepticus, we accurately predicted the frequency of SRS ($R = 0.92$; $R^2 = 0.86$; $P < 0.0001$) at the onset of epilepsy. This study not only demonstrates non-invasive imaging of translocator protein as a prognostic biomarker to ascertain SRS frequency, but also shows its capability to reflect the severity of depression-like and sensorimotor-related comorbidities. Our results are an encouraging step towards the development of anti-epileptogenic treatments by

providing early quantitative assessment of SRS frequency and severity of comorbidities with high clinical relevance.

**Keywords:** Epileptogenesis; translocator protein; PET; biomarker; comorbidity; spontaneous recurrent seizures

**Abbreviations:**

SRS = spontaneous recurrent seizures

TSPO = translocator protein

PET = positron emission tomography

SE = status epilepticus

KA = kainic acid

KASE = kainic acid-induced status epilepticus

PED = periodic epileptiform discharge

vEEG = video-electroencephalography

SUV = standardized uptake value

PCA = principal component analysis

PLS = partial least squares

VOI = volume of interest

WNT = whisker nuisance task

SPT = sucrose preference test

FST = forced swim test

$SO_2$ = oxygen saturation

## 1. Introduction

Epilepsy is one of the most common chronic neurological disorders, with an estimated prevalence of nearly 65 million people worldwide (Ngugi et al., 2010). It is characterized by the occurrence of spontaneous recurrent seizures (SRS) and a high prevalence of comorbid medical disorders resulting in a devastating impact on patient's daily life (Keezer et al., 2016). Temporal lobe epilepsy accounts for approximately 60% of all partial epilepsies, which makes it the most common form of focal and often refractory epilepsy that can occur during adulthood (Tellez-Zenteno and Hernandez-Ronquillo, 2012). Over the last 40 years no progress has been made in preventing new-onset epilepsy or stopping the significant rise of cases in the elderly population (Sillanpaa et al., 2016). The medicinal therapies available are purely symptomatic, they can have unwanted cognitive or neurobehavioral side effects, and they are ineffective in up to 30% of patients with epilepsy (Kwan and Brodie, 2000), resulting in poor quality of life (Pugliatti et al., 2007). As a consequence, both the prediction and prevention of epilepsy are important public health issues and require urgent attention. In this regard, there is a pressing need to develop biomarkers reflecting disease outcome. These biomarkers will increase our understanding of epileptogenesis and enable early detection and treatment of epilepsy and its comorbidities (Pitkanen et al., 2016).

Several studies have confirmed increased brain inflammation in animal models during epileptogenesis (Amhaoul et al., 2015; Auvin et al., 2010; Brackhan et al., 2016; Dedeurwaerdere et al., 2012a; Pernot et al., 2011; Walker et al., 2016). Pitkanen and Engel (2014) defined epileptogenesis as "the development and extension of tissue capable of generating spontaneous seizures, resulting in a) development of an epileptic condition and/or b) progression of the epilepsy after it is established". Inflammation is recognized to be an important factor in epileptogenesis, offering a new target for the development of anti-epileptogenic therapies and prognostic tools (Dedeurwaerdere et al., 2012b; Ravizza et al., 2011; Vezzani et al., 2013; Vezzani and Friedman, 2011). Radiotracers targeting the translocator protein (18 kDa) (TSPO) serve as an *in vivo* positron

emission tomography (PET) biomarker of inflammation and activated microglia. Recent studies indicated that PET imaging of brain inflammation could be used as a tool to investigate drug resistance in chronic epilepsy (Bogdanovic et al., 2014; Syvanen et al., 2013). As TSPO has been shown to be upregulated in patients with epilepsy (Gershen et al., 2015; Hirvonen et al., 2012; Vezzani and Friedman, 2011), as well as in animal models (Amhaoul et al., 2015; Brackhan et al., 2016; Dedeurwaerdere et al., 2012a), it could represent a valid *in vivo* biomarker for epilepsy. In addition, alterations in its expression have been associated with different psychiatric disorders (Rupprecht et al., 2009; Setiawan et al., 2015).

The development of second-generation tracers targeting TSPO with enhanced pharmacological and pharmacokinetic properties (e.g. [$^{18}$F]-PBR111 and [$^{18}$F]-DPA-714), offer an appropriate tool for translational *in vivo* PET imaging. We previously showed the increased uptake of TSPO PET ligand [$^{18}$F]-PBR111 in the hippocampus and temporal lobe of kainic acid-induced status epilepticus (KASE) rats in the first weeks following status epilepticus (SE) (Amhaoul et al., 2015; Dedeurwaerdere et al., 2012a). An increased uptake of the PET ligand [$^{18}$F]-DPA714 has also been reported following SE and stroke (Harhausen et al., 2013), with the evaluation of the temporal distribution profile using TSPO radioligands showing a peak at 2 weeks post-SE (Amhaoul et al., 2015; Brackhan et al., 2016). Recently, we have demonstrated a correlation between TSPO expression during chronic epilepsy and the occurrence of SRS (Amhaoul et al., 2015). In addition, it has been reported that patients with major depressive episodes have increased TSPO levels (Setiawan et al., 2015). In summary, there seems to be a link between TSPO during epileptogenesis and seizure occurrence, as well as the development of comorbid disorders. However, no longitudinal *in vivo* imaging study evaluating this possible link has yet been performed.

On this basis we investigated whether *in vivo* neuroimaging of inflammation by means of [$^{18}$F]-PBR111 TSPO PET at disease onset (2w post-SE) as well as at established disease (4w post-SE) was predictive of epilepsy severity (SRS frequency) and associated depression-like and

sensorimotor-related comorbidities in KASE rats. Animals were scanned at the onset of epilepsy to offer a stronger translational significance to this study. For the purpose of our work, we selected the KASE rat model of temporal lobe epilepsy, a well-established model characterized by SRS acquired after SE (Amhaoul et al., 2015; Drexel et al., 2012; Levesque and Avoli, 2013), behavioral abnormalities (Inostroza et al., 2012; Levesque and Avoli, 2013; Mazarati et al., 2008) and poor response to antiepileptic drugs (Loscher and Brandt, 2010). This model recapitulates several key features of human temporal lobe epilepsy, the most common and refractory form of focal, acquired epilepsy in adults (Lothman et al., 1991).

## 2. Materials and methods

### 2.1 Animals

Five-week-old male Wistar Han rats (Charles River Laboratories, France) were individually housed under a 12 h light/dark cycle in a temperature and humidity controlled environment with food and water available *ad libitum*. The animals were acclimatized for 6 days before the start of procedures, which were performed according to the European Committee guidelines (decree 86/609/CEE) and the Animal Welfare Act (7 USC 2131). All of the experiments were approved by the Ethical Committee for Animal Testing (ECD 2014-39) at the University of Antwerp (Belgium).

### 2.2 Experimental design

A total of 24 rats were included in the study, of which 18 were induced with kainic acid and six were included as control animals. All animals were implanted with MRI-compatible epidural electrodes 2 weeks before induction of SE and were monitored continuously (24/7) with video-electroencephalography (vEEG) during all stages of the disease (acute, latent and chronic epilepsy) for the entire study (12 weeks) in order to assess the SRS frequency for each subject. To evaluate whether early TSPO expression could predict SRS frequency and comorbidities, the rats were scanned at two different points in time during epileptogenesis (14 and 28 days post-SE, disease onset and established disease, respectively) (Supplementary Fig. 1) with a non-invasive protocol by means of [$^{18}$F]-PBR111 PET imaging, as previously described by our group (Amhaoul et al., 2015; Dedeurwaerdere et al., 2012a). Magnetic resonance imaging (MRI) scans were acquired in parallel with PET scans to evaluate volumetric changes, as well as for co-registration purposes (Amhaoul et al., 2015). Depression-like and sensorimotor-related comorbidities were determined during chronic epilepsy using the whisker nuisance task (WNT, 9 and 11 weeks post-SE), the sugar preference test (SPT, 12 weeks post-SE) and the forced swim test (FST, 12 weeks post-SE).

### 2.3 Electrode implantation

The implantation of the electrodes was performed as previously described (Amhaoul et al., 2015) 2 weeks before the start of the vEEG recordings, allowing an adequate recovery period. A brief description of the procedure is provided in the Supplementary data.

### 2.4 Status epilepticus induction

Two weeks after electrode implantation, the animals were repeatedly administered low-dose injections of kainic acid (KA), as this method has proven its efficacy and has a low mortality rate (Dedeurwaerdere et al., 2012a). At SE induction, the rats were aged 7.5 weeks, with an average weight of 231 ± 7.39 g. The KASE rats were injected s.c. with an initial dose of 7.5 mg/kg KA (A.G. Scientific, USA) and after 1 h, repetitive injections of 2.5 mg/kg were given every half-hour unless the animal showed seizure behavior. Injections were repeated until the animals displayed convulsive seizures. All animals reached SE (100% induction rate) after receiving an average dose of 20.15 ± 1.38 mg/kg of KA and only one rat did not survive the procedure (6% mortality rate). During the entire period, the animals were continuously observed and after 4 h of SE, diazepam (4 mg/kg; NV Roche SA, Belgium) was administered intraperitoneally (i.p.) to reduce seizures. Control animals received only saline injections (range of 4–6 injections). At the end of the procedure, Hartmann's solution (10 ml/kg, s.c.) was administered to prevent dehydration. Additional care was taken in the days following SE, with the animals receiving enriched soft food pellets and Hartmann's solution (10 ml/kg, s.c.).

After 4h of observation of SE, the animals were connected to the vEEG system. KASE rats displayed electrographic seizures evolving in continuous spiking activity. A decrease in spiking frequency and the disappearance of discharges was observed at the time of the transition from

continuous electrographic ictal activity to high-frequency, high-amplitude periodic epileptiform discharges (PEDs) with temporary spike activity. We considered the SE terminated only when the last PED occurred (Van Nieuwenhuyse et al., 2015).

## 2.5 vEEG recording and analysis

A total of 12 weeks of vEEG data were collected from freely moving animals. All control and KASE rats were subjected to continuous vEEG for the recording period. The epidural electrode assembly was connected to the digital EEG acquisition system (Ponemah P3 Plus; Data Sciences International, USA) using a three-channel connector cable with a spring and a rotor-containing commutator (Bilaney Consultants, Plastic One Inc., Germany), as previously described (Amhaoul et al., 2016). Synchronized video images were recorded with a network video camera (Axis P1343, Axis Communications, Sweden), and a night-vision infrared lamp (Raymax 25 IP, Raytec, UK) was used to ameliorate video quality during the lights-off period. An experienced investigator constantly monitored the animals when they were uncoupled from the vEEG setup for scanning or behavioral tests. A total of 10 SRS were documented during these intervals.

Analysis of vEEG recordings was performed manually using Neuroscore 3.0 (Data Sciences International, USA) by an experienced investigator. The identification of SRS was executed as previously described (Amhaoul et al., 2016). Briefly, the amplitude of the signal must be at least three times the baseline signal (awake), the frequency of the signal must be at least two times the baseline signal, and the aberrant EEG-tracing must persist for at least five seconds (Williams et al., 2009) (Supplementary Fig. 2E and 2F). In addition, to be classified as epileptic activity, video-recordings were used to visually determine the severity of the SRS according to the modified scale of Racine (Amhaoul et al., 2016; Racine, 1972). The duration of SE, the latency to the first SRS, the

duration of SRS, the circadian rhythm of SRS, the temporal evolution of SRS, and the total number of SRS (seizure burden) were determined.

## 2.6 *In vivo* imaging

### 2.6.1 [$^{18}$F]-PBR111 PET imaging

[$^{18}$F]-PBR111 radiosynthesis was performed on a Fluorsynton I automated synthesis module (Comecer Netherlands, the Netherlands) according to Bourdier and colleagues (2012). PET scans were performed on an Inveon PET/Computed Tomography (CT) scanner (Siemens Preclinical Solution, USA). Physiological monitoring was performed as previously described (Dedeurwaerdere et al., 2012a). The rats were anaesthetized using isoflurane (Forene, Belgium) in medical oxygen (induction 5%, maintenance 2-2.5%). Respiration rate and body temperature of the animal were constantly monitored (Minerve, France) during the entire scanning period and they were in the acceptable range during the scan (respiration rate = 60.2 ± 2.1 breaths/min). The core body temperature of the animals was maintained at 37 ± 0.5 ºC via a temperature-controlled heating pad. The radiotracer (injected dose 8.3 ± 2.7 MBq, specific activity 209.8 ± 21.4 GBq/μmol, cold mass 0.104 ± 0.017 nmol or 0.35 nmol/kg in a volume of 0.5 ml) was administered into the tail vein over a duration of 1 min, using an automated pump (Pump 11 Elite, Harvard Apparatus, USA) and a glass syringe (Model 1001 LT SYR, Hamilton Company, USA) (Amhaoul et al., 2015). Brain distribution of TSPO ligand [$^{18}$F]-PBR111 was measured by a 15 min static scan 45 min after the injection of the radiotracer. After the PET scan, a 10 min 80 kV/500 μA CT scan was performed for attenuation correction and for co-registration of the PET images to the MRI data. Iterative PET image reconstruction was performed after Fourier rebinning (Defrise et al., 1997) using an ordered-subset expectation maximization algorithm (OSEM-2D) (Hudson and Larkin, 1994) with corrections for dead-time, attenuation and random coincidences provided by the manufacturer.

Standardized uptake values (SUVs) representing the ratio of tissue uptake and injected radioligand dose normalized by the body weight of each individual animal were determined. The timing window (45-60 min p.i. of [$^{18}$F]-PBR111) for imaging was determined from the time activity curves (TACs) from a previous study showing that [$^{18}$F]-PBR111 uptake remains stable during this period (Dedeurwaerdere et al., 2012a). Moreover, the reliability of the SUVs was evaluated based on these data showing robust correlations between the SUVs and total volume of distribution (Vt) values (Supplementary Fig. 3 and Supplementary Table 1). In addition, there was no difference in metabolisation of the tracer between controls and KASE rats (controls = 12.66 ± 0.95 % parent compound; KASE rats = 13.19 ± 0.56 % parent compound).

Two PET scans at the 2 weeks post-SE time point were aborted because of a faulty tracer injection (KASE 4) or CT failure (KASE 8). These rats were scanned 4 weeks post-SE, but they were excluded from the PET analysis.

**2.6.2. $T_2$ MRI**

In the same week as the PET/CT scans, MRI scans were performed as previously described (Amhaoul et al., 2015). The animals were anaesthetized using isoflurane (Forene, Belgium) in a mixture of $N_2/O_2$ (induction 5%, maintenance 2.5%) and placed in prone position into the scanner (9.4T Biospec, Bruker, Germany) with the head fixed in a head holder. A rectal thermistor was inserted to monitor the body temperature, which was maintained at 37 ± 0.5 ºC by means of a feedback-controlled warm air circuitry (MR-compatible Small Animal Heating System, SA Instruments, Inc., USA). Blood oxygen saturation ($SO_2$) and respiration rate were monitored throughout the experiment using a pulse oximeter and a pressure sensitive sensor under the rat (MR-compatible Small Animal Monitoring and Gating System, SA Instruments, Inc., USA) and they were in the acceptable range during the scan ($SO_2$ = 97.1 ± 0.8%; respiration rate = 61 ± 1.4 breaths/min). After a Tripilot scout image, a rapid acquisition with relaxation enhancement (RARE) sequence was used to obtain 70 coronal slices with a 0.4 mm thickness (0.17 x 0.114 x 0.35 mm

voxels), an acquisition matrix of 256 x 344, and a field of view (FOV) of 30 x 40 x 28 $mm^2$. The MR image acquisition procedure lasted for about 10 min, after which the animals were placed in a recovery box while heated under an infrared lamp. All data were acquired using ParaVision 5.1 (Bruker, Germany).

#### 2.6.3. Data analyses

Co-registration of PET and MRI was achieved by automated rigid matching of CT to MR images using PMOD version 3.3 (PMOD Technologies, Switzerland). Given the sequential acquisition of PET and CT on the same bed, the CT to MR rigid transformation was used to overlay the PET and MR images. Volumes of interest (VOIs) were manually delineated on the individual MR images for each animal in PMOD (PMOD Technologies, Switzerland). The different VOIs included the olfactory bulb, the frontal cortex, the hippocampus, the extrahippocampal temporal lobe, the insular cortex, the anterior piriform cortex, the thalamus, the hypothalamus, the ventricles and the cerebellum. Volumetric assessment of the brain regions investigated was performed by normalizing each VOI to the whole brain volume.

### 2.7 Comorbidities assessment

All behavioral tasks were performed by researchers blinded to experimental conditions using standardized tests (Mazarati et al., 2008; McNamara et al., 2010; Porsolt et al., 1979; Vloeberghs et al., 2007) as summarized in Supplementary Fig. 1.

#### 2.7.1 Whisker nuisance task

The whisker nuisance task (WNT) measures an animal's behavioral response to somatosensory cortex activation via whisker stimulation to determine altered neuropsychological functions. In addition, the scoring of this task takes into consideration anxiety, aggressiveness and the

exploratory behavior of the animals (McNamara et al., 2010). The test was performed 9 and 11 weeks post-SE in controls ($n$ = 3) and KASE ($n$ = 12) rats. Briefly, the rats were acclimatized in a plastic test cage lined with an absorbent pad. The whiskers were manually stimulated with a wooden applicator stick for three consecutive 5 min periods, between which the animals were observed for 1 min. Behavioral scoring was conducted by 2 blinded observers. High scores (8-16) indicate an abnormal response to the stimulation (e.g. rat freezes, becomes agitated or aggressive), while low scores (0-4) indicate normal responses (McNamara et al., 2010). At the end of the task, the animals were reconnected to the vEEG monitoring system. One animal was excluded from the analysis due to experiencing a SRS during the test (KASE 14).

### 2.7.2 Sucrose preference test

A sucrose preference test (SPT) was performed to evaluate anhedonic behavior in KASE rats during chronic epilepsy. During the final week of vEEG monitoring (12 weeks post-SE), controls ($n$ = 3) and KASE ($n$ = 13) rats were supplied with two identical water bottles, one with 2% sucrose and the other without, in the presence of *ad libitum* food. Every day the position of the bottles was exchanged and the consumption from each bottle measured (Vloeberghs et al., 2007). After a 48 h period of habituation to avoid bias due to neophobia, the two bottles were again placed in the cage and the consumption from each was recorded after a 24 h interval. The preference for sucrose was calculated as the relative amount of water with sucrose versus total liquid (water with and without sucrose) consumed by the rats. Two animals were excluded from the analysis due to a liquid consumption of more than the average of other animals plus 2 standard deviations (2.4-fold and 1.9-fold higher consumption compared to the average of controls and KASE rats, i.e. 64.5 ± 7.8 ml, KASE 2 and KASE 4 respectively).

### 2.7.3 Forced swim test

Forced swim test (FST) was performed to determine depressive-like behavior. We employed a modified version of the classic FST, in which the animals (controls $n$ = 6; and KASE rats $n$ = 15) underwent a single 5 min trial. This modification of the Porsolt protocol (Porsolt et al., 1979) has been described as relevant to examining depressive-like behavior (Mazarati et al., 2008). Only a single trial test before sacrifice was possible because the exposure of the electrode assembly to water may disrupt its functioning. The animals were placed for 5 min in a glass cylinder (65 cm in height, 25 cm in width) that was filled with tap water to a height of 50 cm and maintained at 25-26°C. After each test, the cylinder was washed and refilled with fresh water. Tests were videotaped and analyzed blinded to treatment. 'Time of immobility' was defined as the time the animal stopped swimming and only used minimal movements to keep its head above water. 'Swimming' was defined as roaming around in the water using synchronized paw movements, and 'climbing' as upward-directed forceful movements with all paws.

## 2.8 Data-driven modeling of brain inflammation

### 2.8.1. Principal component analysis

Principal Component Analysis (PCA) is a data reduction method that determines a set of linearly uncorrelated components that account for variability in a dataset. In this study, PCA was applied to the [$^{18}$F]-PBR111 SUV in the different VOIs of the different animals at 2 and 4 weeks post-SE in order to identify different patterns of brain uptake across the animals. A total of 10 dimensions were determined and two dimensions were extracted. Factor loadings on each extracted factor were used to calculate contributions derived from each VOI. PCA was performed in R (version 3.2.2), using the *factoextra* package. To perform a valid PCA, no guide is given on the number of observations needed; however to obtain satisfactory results a subjects-to-variables ratio of 1.2 is required (Barrett

and Kline, 1981). In our study, the subject-to-variable ratio was 2.1, and therefore our sample size seemed adequate for the purposes of PCA.

### 2.8.2. Partial least squares regression

Partial least squares (PLS) regression is a method for constructing predictive models when there are many highly collinear factors (SUVs for different VOIs). It is based both on a regression of the independent variables (factors; VOIs) on the dependent variable (response; SRS/day) and vice versa (Naes and Martens, 1985).

In this study, PLS regression was applied to the [$^{18}$F]-PBR111 uptake of the different VOIs. Only KASE rats were included in the analysis since the goal was to predict SRS frequency for each subject. A quasi-Poisson distribution was used to account for count data and overdispersion. The optimal number of components was obtained by cross validation (Gomez-Carracedo et al., 2007). Confidence intervals for the regression coefficients were determined by antithetic bootstrapping (Afanador et al., 2013). PLS regression was performed in R (version 3.2.2), using the *pls* package.

## 2.9 Statistical analysis

All analyses were performed by blinded observers. All data were assessed for normality (Shapiro-Wilk test). No evidence against normality was found, except for the number of SRS. However, given the sample size of the control group ($n$ = 6), a Mann-Whitney U test was used to determine differences between the control and KASE animals at each time point for all *in vivo* variables. A Wilcoxon signed rank test was used to evaluate the circadian rhythm of SRS. WNT scores were compared by two-way repeated-measures ANOVA, while the Mann-Whitney U test was used for SPT and FST. A Kruskal-Wallis test with post-hoc Dunn's multiple comparison test was used to compare SRS for the different categories of KASE rats. Spearman's rank correlation test was used to examine the relationship between SRS and all variables in the KASE animals. To investigate

whether a relationship existed between the TSPO PET or MRI data and the behavioral outcomes, as well as between the PET SUVs and Vt values, Pearson's correlation test was used. All of the above-mentioned analyses were performed with GraphPad Prism (v 6.0) statistical software. The data are represented by means ± standard error mean (s.e.m.). All tests were two-tailed and significance was set at $P < 0.05$.

# 3. Results

## 3.1 Temporal profile of SRS following SE

The mean duration of SE was 15.07 ± 0.92 h (Supplementary Fig. 2A). The mean latency to the first SRS was 22.30 ± 3 days (Supplementary Fig. 2B), while the median was 15.51 days. On average, KASE rats experienced 0.32 ± 0.06 SRS per day (in a range of 0.00 – 0.83 SRS/day). All electrographic seizures were convulsive (mostly class 4); this was visually confirmed by matching the time-locked video recordings. The analysis showed that 2 out of 17 KASE rats (12%) did not experience SRS during the whole study. The average duration of SRS was 39.87 ± 0.55 s (Supplementary Fig. 2C). In addition, a circadian rhythm was identified: the average number of SRS during the lights-on phase was 16.60 ± 4.06 SRS per animal, whereas the seizure burden during the lights-off phase was significantly lower, at 3.80 ± 1.30 SRS per animal ($P < 0.0001$) (Supplementary Fig. 2D). The evolution profile of the SRS during the 12 weeks recorded, as well as the total number of SRS experienced by each animal (range of 0 – 68 SRS) during the whole recording period were also determined (Supplementary Fig. 2G, 2H).

## 3.2 *In vivo* imaging of TSPO expression and volumetric changes during epileptogenesis

*In vivo* TSPO expression in the brain was determined by means of a longitudinal [$^{18}$F]-PBR111 PET scan at 2 and 4 weeks post-SE. The binding of the TSPO ligand [$^{18}$F]-PBR111 2 weeks post-SE was significantly increased in KASE rats across the whole limbic system compared to controls (Fig. 1A): the hippocampus and the temporal lobe ($P < 0.0001$), the ventricles ($P < 0.001$), the thalamus and the hypothalamus ($P < 0.01$), and the insular cortex ($P < 0.05$). High tracer binding was also seen in the anterior piriform cortex ($P = 0.066$), although it was not statistically significant. There

were no significant differences in olfactory bulb, frontal cortex or cerebellum between the control and KASE rats.

The binding of [$^{18}$F]-PBR111 4 weeks post-SE was significantly increased in KASE rats in the temporal lobe ($P < 0.01$), the hippocampus and the thalamus ($P < 0.05$) compared to controls (Fig. 1B). There were no significant differences in the remaining regions between the control and KASE rats.

Volumetric assessment of the different brain regions based on MR images showed hippocampal volume reduction 2 weeks post-SE (decreased by 16%; $P < 0.01$) in KASE animals compared to controls (Fig. 1C). No significant volumetric changes were found in the remaining VOIs investigated.

MR images 4 weeks post-SE displayed a progressive reduction in hippocampal volume (decreased by 22%; $P < 0.01$), and showed a significant ventricular enlargement (increased by 50%; $P < 0.05$) in KASE animals compared to controls (Fig. 1D). No significant volumetric alterations were found in the residual VOIs.

### 3.3 KASE rats display comorbidities during chronic epilepsy

Alterations of the somatosensory whisker function were assessed using the WNT at the 9 and 11 weeks post-SE. KASE rats displayed altered behavior 9 weeks post-SE (controls = 1.81 ± 1.10 score; KASE rats = 7.42 ± 0.62 score, $P = 0.0016$) as well as at 11 weeks post-SE (controls = 2.70 ± 1.26 score; KASE rats = 7.18 ± 0.64 score, $P = 0.0103$) compared to the controls (Fig. 2A, 2D respectively). The inter-rater reliability was consistent both for 9 weeks post-SE ($R^2 = 0.569$; $P < 0.0001$) and 11 weeks post-SE ($R^2 = 0.645$; $P < 0.0001$).

Anhedonic behavior was assessed using a 24 h sucrose preference test 12 weeks post-SE. It was found that the KASE rats had reduced preference for sucrose compared to the control animals (controls = 97.51 ± 0.74 %; KASE rats = 91.16 ± 1.55 %, $P = 0.004$) (Fig. 2G).

Finally, behavioral despair was assessed using the FST 12 weeks post-SE. KASE rats spent a significantly longer time in an immobile state compared to the control animals ($P = 0.0267$) (Fig. 2J). Consistent with the increased immobility displayed, KASE rats spent a lower amount of time climbing (controls = 118.30 ± 8.72 sec; KASE rats = 75.67 ± 12.77 sec, $P = 0.0827$), while no difference in swimming time was detected (controls = 122.50 ± 12.43 sec; KASE rats = 116.00 ± 10.09 sec, $P = 0.7733$). All behavioral scores are summarized in Supplementary Table 2.

### 3.4 Brain inflammation during epileptogenesis reflects chronic comorbidities

Behavioral outcomes during chronic epilepsy correlated with [$^{18}$F]-PBR111 uptake at disease onset and at established disease, as represented in Fig. 2 and Table 1: comorbid behavior during WNT 9 and 11 weeks post-SE correlated with higher [$^{18}$F]-PBR111 uptake in the limbic structures shown in PET imaging at 2 weeks post-SE (hippocampus: R = 0.87, $P < 0.0001$, Fig. 2B; and R = 0.76, $P < 0.01$, Fig. 2E) and in PET imaging at 4 weeks post-SE (hippocampus: R = 0.67, $P < 0.01$, Fig. 2C; and R = 0.73, $P < 0.01$ Fig. 2F). In addition, [$^{18}$F]-PBR111 uptake at 2 and 4 weeks post-SE correlated with reduced sucrose preference (hippocampus: R = -0.76, $P < 0.01$, Fig. 2H and R = -0.81, $P < 0.001$, Fig. 2I). Furthermore, longer immobility time during FST was observed in subjects with higher [$^{18}$F]-PBR111 uptake at 2 and 4 weeks post-SE (hippocampus: R = 0.54, $P < 0.05$, Fig. 2K and R = 0.63, $P < 0.01$, Fig. 2L). No correlation was found between behavioral outcomes and SRS or volumetric changes ($-0.23 < R < 0.35$, $P > 0.05$ for all pairs of variables).

### 3.5 Data-driven modeling of brain inflammation predicts SRS frequency

The [$^{18}$F]-PBR111 uptake in any of the individual VOIs did not correlate with SRS frequency for any VOI investigated (-0.38 < R < +0.32, $P$ > 0.05 for all pairs of variables). Given the multidimensionality of the TSPO PET imaging data, we applied PCA to simplify the representation of the variability in the dataset. PCA based on TSPO PET imaging 2 weeks post-SE produced a two-dimensional outcome, which accounted for 80% of the variance in the PET data (Dim1 = 66.6%; Dim2 = 13.4%) (Fig. 3A). The temporal lobe and hippocampus were the most relevant regions for explaining PCA variability (Fig. 3B). In addition, we could identify three different categories of KASE animals according to PCA and SRS frequency and were accordingly named "absent or rare SRS", "sporadic SRS" and "frequent SRS" (Fig. 3A, 3C). The absent or rare SRS (1.50 ± 0.86 SRS) category exhibited a significantly lower number of SRS compared to the frequent SRS category (47.25 ± 7.84 SRS) ($P$ < 0.01). No significance difference was found between the sporadic SRS (15.30 ± 1.88 SRS) and frequent SRS categories ($P$ = 0.14) or between absent or rare SRS and sporadic SRS ($P$ = 0.14).

PCA based on TSPO PET data 4 weeks post-SE could not determine any difference among subjects (Supplementary Fig. 4A).

In order to construct a predictive model of SRS frequency in KASE animals, we applied PLS regression on TSPO PET imaging. PLS regression based on TSPO PET imaging 2 weeks post-SE generated a predictive model (R = 0.92; $R^2$= 0.86; $P$ < 0.0001) (Fig. 3D). In line with the PCA, a model with two components resulted in the best fit (Fig. 3B) and the temporal lobe and hippocampus were the most relevant VOIs for explaining the PLS prediction outcome. The PLS model was able to predict SRS frequency with high accuracy based on the 2-week PET scan acquired before the animals had chronic epilepsy. As a result, PLS regression enabled us to determine the SRS frequency for every subject before epilepsy was acquired based on a single non-invasive TSPO PET scan.

The PLS regression model lost predictive strength when using the TSPO PET data 4 weeks post-SE ($R = 0.71$; $R^2 = 0.44$; $P < 0.01$) (Supplementary Fig. 4C).

## 4. Discussion

The impact of comorbidities on the quality of life of patients has been underestimated (Keezer et al., 2016). The development of comorbidities in epilepsy may cause greater impairment in the quality of life than seizures (Keezer et al., 2016). Nevertheless, relatively little progress has been made in identifying biomarkers and developing new therapies directed specifically at comorbidities (Brooks-Kayal et al., 2013). We found that regional TSPO PET imaging at disease onset and at established disease correlated with depression-like and somatosensory-related comorbidities during chronic epilepsy (Fig. 2 and Table 1). The evidence that higher TSPO levels correlate with the severity of depressive-like behavior is consistent with the concept that neuroinflammation may contribute to sickness behavior. This is supported by previous findings in which patients with mild-to-moderate depression had TSPO levels in the brain similar to healthy subjects (Hannestad et al., 2013), whereas individuals with severe major depressive episodes had higher TSPO levels in the brain than control subjects (Setiawan et al., 2015). Notably, SRS frequency was not a determinant of the extent of comorbidities, as previously reported in patients with temporal lobe epilepsy (Gilliam et al., 2007). While we cannot exclude the possibility that KASE rats had already developed comorbid behavior during early phases of the disease, to our knowledge only one study has reported a trend for KASE rats to be less mobile during FST in the early stage of the disease (Koh et al., 2007). Nevertheless, our finding that regional TSPO PET imaging during epileptogenesis correlates the clinical manifestation of comorbidities suggests for the first time a symptomatic biomarker for depression-like and sensorimotor-related comorbidities. This finding is clinically relevant and could be of value for developing new treatments.

We have also shown for the first time the capability of a single PET scan, acquired 2 weeks post-SE to accurately predict SRS frequency by means of data-driven modeling of brain inflammation at onset of epilepsy (Fig. 3A and 3D). To date, the analysis of TSPO PET imaging has been oriented towards alterations in separate brain regions, describing increases or decreases in tracer binding

without providing insight into alterations of the brain network during epileptogenesis (Brackhan et al., 2016; Dedeurwaerdere et al., 2012a; Harhausen et al., 2013; Toth et al., 2016; Vallez Garcia et al., 2015). Taking into account the importance of brain networks in epilepsy, we believe that crucial information lies in the 3D region-interdependent changes in the brain. Indeed, differences in regional [$^{18}$F]-PBR111 uptake at disease onset and at established disease did not reflect SRS frequency, suggesting that single VOIs are not informative enough to explain the development of SRS. However, the data-driven modeling of brain inflammation presented here overcomes the limitations of a single region analysis and examines PET uptake variations in different regions at the same time, thus considering the whole brain network. This method reveals that during epileptogenesis brain inflammation is not present in different brain regions independently, and interactions between regions appear to be relevant to the prediction of SRS frequency. Hence, by shifting away from a categorical analysis of the PET data towards a continuous multi-dimensional characterization, more graded aspects of disease ontogenesis were captured. As a result, we were able to accurately predict SRS frequency for each subject based on a single non-invasive TSPO PET scan at onset of epilepsy. Notably, the most relevant regions that best explain the SRS outcome were the temporal lobe and the hippocampus (Fig. 3B), regions well known to be involved in seizure generation and spread. Interestingly, the data-driven modeling was able to predict SRS frequency based on [$^{18}$F]-PBR111 uptake 2 weeks post-SE (Fig. 3A and 3D), when the first seizures were starting to occur (Supplementary Fig. 2B). This time point coincides with the first SRS and therefore represents a clinical significant stage to evaluate the disease also in patients. The high predictive value of the 2 weeks post-SE time point is because of the elevated level of inflammation occurring into the brain, while the loss of predictive strength 4 weeks post-SE is due to the resolving of brain inflammation taking place at this time point.

In this animal model of TLE, we observed depression-like and sensorimotor-related comorbidities as well as SRS during chronic epilepsy. The capability of *in vivo* imaging of brain inflammation to

reflect the severity of the comorbidities and to predict SRS, suggest a link between brain inflammation with the investigated comorbidities and SRS. Two key mechanisms associated to depression, namely a reduced serotonergic transmission from raphe nucleus into afferent projections (such as to the neocortex and hippocampus) and a dysregulation of the hypothalamo-pituitary-adrenocortical axis, have been reported to be altered in rats following SE (Mazarati et al., 2008; Mazarati et al., 2009). Interestingly, epilepsy-related depression can be alleviated when targeting brain inflammation, such as by infusion of recombinant interleukin-1 receptor antagonist (Mazarati et al., 2010). These findings recommend that depression may, at least in part, result from increased brain inflammation, which may explain the direct relationship we found between brain inflammation and the severity of the depression-like behavior. On the contrary, epilepsy severity (defined by SRS frequency) did not directly correlate with TSPO binding at epilepsy onset. SRS are not the result of alterations in a single pathway, but they are the consequence of the composite changes of more complex phenomena, which in addition involves interplay between several brain areas and their projections. When considering the whole brain network, we could identify a relationship between brain inflammation at epilepsy onset and SRS frequency. Several processes are involved in the hyperexcitability mediated by inflammation. The mechanisms underlying the proconvulsant effects of released cytokines, such as interleukin-1β and High Mobility Group Box 1, include enhanced N-methyl-$_D$-aspartate-mediated inward $Ca^{2+}$ currents (Viviani et al., 2003) and increased neuronal synaptic expression of AMPA receptors more permeable to $Ca^{2+}$ mediated by TNF-α (Beattie et al., 2002). In addition, TNF-α reduces inhibitory synaptic strength by inducing endocytosis of $GABA_A$ receptors (Stellwagen et al., 2005). Furthermore, pro-inflammatory cytokines can also increase the extracellular glutamate concentration by reducing astrocytic glutamate reuptake (Hu et al., 2000). Inflammatory mediators may also trigger transcriptional changes, which could promote chronic inflammation and expression of genes involved in neurogenesis, cell death, and molecular and synaptic plasticity (O'Neill and Bowie, 2007; Vezzani et al., 2011). Finally, inflammatory molecules may contribute to blood-brain barrier breakdown

resulting in parenchymal accumulation of serum albumin, which can induce long lasting hyperexcitability by impairing astrocyte ability to buffer potassium and glutamate (Friedman et al., 2009). Altogether, these molecular changes may contribute to the severity of epilepsy. Although it seems that globally epilepsy severity does not correlate with the severity of depression-like behavior, it is important to underline that SRS can cause brain inflammation and vice-versa (Vezzani et al., 2011), thus seizure-induced inflammation may affect comorbidities during chronic epilepsy.

A major commitment of the field has been the development of disease-modifying treatments to alter or even prevent epileptogenesis (Baulac and Pitkanen, 2008; Galanopoulou et al., 2012; Pitkanen et al., 2016); nevertheless, no anti-epileptogenic drugs are currently on the market. A primary issue in relation to this shortcoming is the selection of subjects to consider for anti-epileptogenic treatment during preclinical (and clinical) evaluation trials. Indeed, a lack of biomarkers to predict SRS frequency and comorbidities in experimental animal models (as well as in humans) is considered a major limiting factor in current anti-epileptogenic studies (Mani et al., 2011; Pitkanen et al., 2016; Pitkanen et al., 2013; Schmidt et al., 2014). Choy and colleagues (2014) have shown the potential of non-invasive imaging to discriminate seizing animals following febrile status epilepticus. However, a biomarker associated with the onset of SRS and comorbidities could be employed in anti-epileptogenic trials to select animals that will develop similar SRS frequency or severity of depression-like and sensorimotor-related comorbidities, reducing variability and hence significantly increasing statistical power. Non-invasive neuroimaging of inflammation could thus play a key role as biomarker in the selection of animals to include in these preclinical trials, reducing trial costs and increasing feasibility.

A limitation of our study is that we did not perform behavioral tests during the first weeks following SE. Since we could not determine when depression-like and sensorimotor-related comorbidities appeared, we cannot establish whether TSPO PET imaging is not only reflecting, but also predicting

the severity of depression-like and sensorimotor-related comorbidities. In addition, our study design did not allow to determine whether TSPO plays a causative role, future *in vivo* studies with specific TSPO inhibitors or transgenic animals could determine whether TSPO might represent a mechanistic biomarker of epilepsy.

In conclusion, our results not only demonstrate PET imaging of brain inflammation to be a valid prognostic biomarker to ascertain SRS frequency, but also to determine the severity of depression-like and sensorimotor-related comorbidities. Because we scanned the animal at the start of the disease onset, our findings have a high clinical relevance.

## Funding

S.D. is supported by Research Foundation Flanders (FWO) funding 1.5.110.14N, 1.5.144.12N and ERA-NET NEURON G.A009.13N, and finally by Queen Elisabeth Medical Foundation (Q.E.M.F.) for Neurosciences. D.B. has a PhD fellowship from the Research Foundation Flanders (FWO, 11W2516N). S.D. and S.S. are supported by the Bijzonder Onderzoeks Fonds (BOF) of the University of Antwerp. A.V.D.L. is supported by the European Union's Seventh Framework Programme under grant agreement number 278850 (INMiND). E.J. has a post-doctoral fellowship from the Research Foundation Flanders (FWO, 12R1917N). E.S. is supported by a Methusalem grant from the universities of Antwerp and Hasselt, awarded to Prof. Herman Goossens and Prof. Geert Molenberghs. N.H. acknowledges support from the University of Antwerp scientific chair in Evidence-Based Vaccinology, financed in 2009-2015 by an unrestricted gift from Pfizer.

## Acknowledgements

The authors would like to thank their colleagues, K. Szewczyk, P. Joye and C. Berghmans for technical laboratory support and assistance, and David Thomae and Thomas Verbrugghen for providing PBR111 precursor.



## Appendix A. Supplementary data

Supplementary data associated with this article can be found in the online version.

## References

Afanador, N.L., Tran, T.N., Buydens, L.M., 2013. Use of the bootstrap and permutation methods for a more robust variable importance in the projection metric for partial least squares regression. Anal Chim Acta 768, 49-56.

Amhaoul, H., Ali, I., Mola, M., Van Eetveldt, A., Szewczyk, K., Missault, S., Bielen, K., Kumar-Singh, S., Rech, J., Lord, B., Ceusters, M., Bhattacharya, A., Dedeurwaerdere, S., 2016. P2X7 receptor antagonism reduces severity of spontaneous seizures in a chronic model of temporal lobe epilepsy. Neuropharmacology.

Amhaoul, H., Hamaide, J., Bertoglio, D., Reichel, S.N., Verhaeghe, J., Geerts, E., Van Dam, D., De Deyn, P.P., Kumar-Singh, S., Katsifis, A., Van Der Linden, A., Staelens, S., Dedeurwaerdere, S., 2015. Brain inflammation in a chronic epilepsy model: Evolving pattern of the translocator protein during epileptogenesis. Neurobiol Dis 82, 526-539.

Auvin, S., Shin, D., Mazarati, A., Sankar, R., 2010. Inflammation induced by LPS enhances epileptogenesis in immature rat and may be partially reversed by IL1RA. Epilepsia 51 Suppl 3, 34-38.

Barrett, P.T., Kline, P., 1981. The observation to variable ratio in factor analysis. . Personality Study in Group Behavior, 23-33.

Baulac, M., Pitkanen, A., 2008. Research priorities in epilepsy for the next decade—A representative view of the European scientific community: Summary of the ILAE Epilepsy Research Workshop, Brussels, 17–18 January 2008. Epilepsia 50, 571-578.

Beattie, E.C., Stellwagen, D., Morishita, W., Bresnahan, J.C., Ha, B.K., Von Zastrow, M., Beattie, M.S., Malenka, R.C., 2002. Control of synaptic strength by glial TNFalpha. Science 295, 2282-2285.

Bogdanovic, R.M., Syvanen, S., Michler, C., Russmann, V., Eriksson, J., Windhorst, A.D., Lammertsma, A.A., de Lange, E.C., Voskuyl, R.A., Potschka, H., 2014. (R)-[11C]PK11195 brain

uptake as a biomarker of inflammation and antiepileptic drug resistance: evaluation in a rat epilepsy model. Neuropharmacology 85, 104-112.

Bourdier, T., Pham, T.Q., Henderson, D., Jackson, T., Lam, P., Izard, M., Katsifis, A., 2012. Automated radiosynthesis of [18F]PBR111 and [18F]PBR102 using the Tracerlab FXFN and Tracerlab MXFDG module for imaging the peripheral benzodiazepine receptor with PET. Appl Radiat Isot 70, 176-183.

Brackhan, M., Bascunana, P., Postema, J.M., Ross, T.L., Bengel, F.M., Bankstahl, M., Bankstahl, J.P., 2016. Serial quantitative TSPO-targeted PET reveals peak microglial activation up to two weeks after an epileptogenic brain insult. J Nucl Med.

Brooks-Kayal, A.R., Bath, K.G., Berg, A.T., Galanopoulou, A.S., Holmes, G.L., Jensen, F.E., Kanner, A.M., O'Brien, T.J., Whittemore, V.H., Winawer, M.R., Patel, M., Scharfman, H.E., 2013. Issues related to symptomatic and disease-modifying treatments affecting cognitive and neuropsychiatric comorbidities of epilepsy. Epilepsia 54 Suppl 4, 44-60.

Choy, M., Dube, C.M., Patterson, K., Barnes, S.R., Maras, P., Blood, A.B., Hasso, A.N., Obenaus, A., Baram, T.Z., 2014. A novel, noninvasive, predictive epilepsy biomarker with clinical potential. J Neurosci 34, 8672-8684.

Dedeurwaerdere, S., Callaghan, P.D., Pham, T., Rahardjo, G.L., Amhaoul, H., Berghofer, P., Quinlivan, M., Mattner, F., Loc'h, C., Katsifis, A., Gregoire, M.C., 2012a. PET imaging of brain inflammation during early epileptogenesis in a rat model of temporal lobe epilepsy. EJNMMI Res 2, 60.

Dedeurwaerdere, S., Friedman, A., Fabene, P.F., Mazarati, A., Murashima, Y.L., Vezzani, A., Baram, T.Z., 2012b. Finding a better drug for epilepsy: antiinflammatory targets. Epilepsia 53, 1113-1118.

Defrise, M., Kinahan, P.E., Townsend, D.W., Michel, C., Sibomana, M., Newport, D.F., 1997. Exact and approximate rebinning algorithms for 3-D PET data. IEEE Trans Med Imaging 16, 145-158.

Drexel, M., Preidt, A.P., Sperk, G., 2012. Sequel of spontaneous seizures after kainic acid-induced status epilepticus and associated neuropathological changes in the subiculum and entorhinal cortex. Neuropharmacology 63, 806-817.

Friedman, A., Kaufer, D., Heinemann, U., 2009. Blood-brain barrier breakdown-inducing astrocytic transformation: novel targets for the prevention of epilepsy. Epilepsy Res 85, 142-149.

Galanopoulou, A.S., Buckmaster, P.S., Staley, K.J., Moshe, S.L., Perucca, E., Engel, J., Jr., Loscher, W., Noebels, J.L., Pitkanen, A., Stables, J., White, H.S., O'Brien, T.J., Simonato, M., American Epilepsy Society Basic Science, C., The International League Against Epilepsy Working Group On Recommendations For Preclinical Epilepsy Drug, D., 2012. Identification of new epilepsy treatments: issues in preclinical methodology. Epilepsia 53, 571-582.

Gershen, L.D., Zanotti-Fregonara, P., Dustin, I.H., Liow, J.S., Hirvonen, J., Kreisl, W.C., Jenko, K.J., Inati, S.K., Fujita, M., Morse, C.L., Brouwer, C., Hong, J.S., Pike, V.W., Zoghbi, S.S., Innis, R.B., Theodore, W.H., 2015. Neuroinflammation in Temporal Lobe Epilepsy Measured Using Positron Emission Tomographic Imaging of Translocator Protein. JAMA Neurol 72, 882-888.

Gilliam, F.G., Maton, B.M., Martin, R.C., Sawrie, S.M., Faught, R.E., Hugg, J.W., Viikinsalo, M., Kuzniecky, R.I., 2007. Hippocampal 1H-MRSI correlates with severity of depression symptoms in temporal lobe epilepsy. Neurology 68, 364-368.

Gomez-Carracedo, M.P., Andrade, J.M., Rutledge, D.N., Faber, N.M., 2007. Selecting the optimum number of partial least squares components for the calibration of attenuated total reflectance-mid-infrared spectra of undesigned kerosene samples. Anal Chim Acta 585, 253-265.

Hannestad, J., DellaGioia, N., Gallezot, J.D., Lim, K., Nabulsi, N., Esterlis, I., Pittman, B., Lee, J.Y., O'Connor, K.C., Pelletier, D., Carson, R.E., 2013. The neuroinflammation marker translocator protein is not elevated in individuals with mild-to-moderate depression: a [(1)(1)C]PBR28 PET study. Brain Behav Immun 33, 131-138.

Harhausen, D., Sudmann, V., Khojasteh, U., Muller, J., Zille, M., Graham, K., Thiele, A., Dyrks, T., Dirnagl, U., Wunder, A., 2013. Specific imaging of inflammation with the 18 kDa translocator protein ligand DPA-714 in animal models of epilepsy and stroke. PLoS One 8, e69529.

Hirvonen, J., Kreisl, W.C., Fujita, M., Dustin, I., Khan, O., Appel, S., Zhang, Y., Morse, C., Pike, V.W., Innis, R.B., Theodore, W.H., 2012. Increased in vivo expression of an inflammatory marker in temporal lobe epilepsy. J Nucl Med 53, 234-240.

Hu, S., Sheng, W.S., Ehrlich, L.C., Peterson, P.K., Chao, C.C., 2000. Cytokine effects on glutamate uptake by human astrocytes. Neuroimmunomodulation 7, 153-159.

Hudson, H.M., Larkin, R.S., 1994. Accelerated image reconstruction using ordered subsets of projection data. IEEE Trans Med Imaging 13, 601-609.

Inostroza, M., Cid, E., Menendez de la Prida, L., Sandi, C., 2012. Different emotional disturbances in two experimental models of temporal lobe epilepsy in rats. PLoS One 7, e38959.

Keezer, M.R., Sisodiya, S.M., Sander, J.W., 2016. Comorbidities of epilepsy: current concepts and future perspectives. Lancet Neurol 15, 106-115.

Koh, S., Magid, R., Chung, H., Stine, C.D., Wilson, D.N., 2007. Depressive behavior and selective down-regulation of serotonin receptor expression after early-life seizures: reversal by environmental enrichment. Epilepsy Behav 10, 26-31.

Kwan, P., Brodie, M.J., 2000. Early identification of refractory epilepsy. N Engl J Med 342, 314-319.

Levesque, M., Avoli, M., 2013. The kainic acid model of temporal lobe epilepsy. Neurosci Biobehav Rev 37, 2887-2899.

Loscher, W., Brandt, C., 2010. High seizure frequency prior to antiepileptic treatment is a predictor of pharmacoresistant epilepsy in a rat model of temporal lobe epilepsy. Epilepsia 51, 89-97.

Lothman, E.W., Bertram, E.H., 3rd, Stringer, J.L., 1991. Functional anatomy of hippocampal seizures. Prog Neurobiol 37, 1-82.

Mani, R., Pollard, J., Dichter, M.A., 2011. Human clinical trails in antiepileptogenesis. Neuroscience Letters 497, 251-256.

Mazarati, A., Siddarth, P., Baldwin, R.A., Shin, D., Caplan, R., Sankar, R., 2008. Depression after status epilepticus: behavioural and biochemical deficits and effects of fluoxetine. Brain 131, 2071-2083.

Mazarati, A.M., Pineda, E., Shin, D., Tio, D., Taylor, A.N., Sankar, R., 2010. Comorbidity between epilepsy and depression: role of hippocampal interleukin-1beta. Neurobiol Dis 37, 461-467.

Mazarati, A.M., Shin, D., Kwon, Y.S., Bragin, A., Pineda, E., Tio, D., Taylor, A.N., Sankar, R., 2009. Elevated plasma corticosterone level and depressive behavior in experimental temporal lobe epilepsy. Neurobiol Dis 34, 457-461.

McNamara, K.C., Lisembee, A.M., Lifshitz, J., 2010. The whisker nuisance task identifies a late-onset, persistent sensory sensitivity in diffuse brain-injured rats. J Neurotrauma 27, 695-706.

Naes, T., Martens, H., 1985. Comparison of prediction methods for multicollinear data. Communications in Statistics - Simulation and Computation 14, 545-576.

Ngugi, A.K., Bottomley, C., Kleinschmidt, I., Sander, J.W., Newton, C.R., 2010. Estimation of the burden of active and life-time epilepsy: a meta-analytic approach. Epilepsia 51, 883-890.

O'Neill, L.A., Bowie, A.G., 2007. The family of five: TIR-domain-containing adaptors in Toll-like receptor signalling. Nat Rev Immunol 7, 353-364.

Pernot, F., Heinrich, C., Barbier, L., Peinnequin, A., Carpentier, P., Dhote, F., Baille, V., Beaup, C., Depaulis, A., Dorandeu, F., 2011. Inflammatory changes during epileptogenesis and spontaneous seizures in a mouse model of mesiotemporal lobe epilepsy. Epilepsia 52, 2315-2325.

Pitkanen, A., Engel, J., Jr., 2014. Past and present definitions of epileptogenesis and its biomarkers. Neurotherapeutics 11, 231-241.

Pitkanen, A., Loscher, W., Vezzani, A., Becker, A.J., Simonato, M., Lukasiuk, K., Grohn, O., Bankstahl, J.P., Friedman, A., Aronica, E., Gorter, J.A., Ravizza, T., Sisodiya, S.M., Kokaia, M.,

Beck, H., 2016. Advances in the development of biomarkers for epilepsy. Lancet Neurol 15, 843-856.

Pitkanen, A., Nehlig, A., Brooks-Kayal, A.R., Dudek, F.E., Friedman, D., Galanopoulou, A.S., Jensen, F.E., Kaminski, R.M., Kapur, J., Klitgaard, H., Loscher, W., Mody, I., Schmidt, D., 2013. Issues related to development of antiepileptogenic therapies. Epilepsia 54 Suppl 4, 35-43.

Porsolt, R.D., Bertin, A., Blavet, N., Deniel, M., Jalfre, M., 1979. Immobility induced by forced swimming in rats: effects of agents which modify central catecholamine and serotonin activity. Eur J Pharmacol 57, 201-210.

Pugliatti, M., Beghi, E., Forsgren, L., Ekman, M., Sobocki, P., 2007. Estimating the cost of epilepsy in Europe: a review with economic modeling. Epilepsia 48, 2224-2233.

Racine, R.J., 1972. Modification of seizure activity by electrical stimulation. II. Motor seizure. Electroencephalogr Clin Neurophysiol 32, 281-294.

Ravizza, T., Balosso, S., Vezzani, A., 2011. Inflammation and prevention of epileptogenesis. Neurosci Lett 497, 223-230.

Rupprecht, R., Rammes, G., Eser, D., Baghai, T.C., Schule, C., Nothdurfter, C., Troxler, T., Gentsch, C., Kalkman, H.O., Chaperon, F., Uzunov, V., McAllister, K.H., Bertaina-Anglade, V., La Rochelle, C.D., Tuerck, D., Floesser, A., Kiese, B., Schumacher, M., Landgraf, R., Holsboer, F., Kucher, K., 2009. Translocator protein (18 kD) as target for anxiolytics without benzodiazepine-like side effects. Science 325, 490-493.

Schmidt, D., Friedman, D., Dichter, M.A., 2014. Anti-epileptogenic clinical trial designs in epilepsy: issues and options. Neurotherapeutics 11, 401-411.

Setiawan, E., Wilson, A.A., Mizrahi, R., Rusjan, P.M., Miler, L., Rajkowska, G., Suridjan, I., Kennedy, J.L., Rekkas, P.V., Houle, S., Meyer, J.H., 2015. Role of translocator protein density, a marker of neuroinflammation, in the brain during major depressive episodes. JAMA Psychiatry 72, 268-275.

Sillanpaa, M., Gissler, M., Schmidt, D., 2016. Efforts in Epilepsy Prevention in the Last 40 Years: Lessons From a Large Nationwide Study. JAMA Neurol 73, 390-395.

Stellwagen, D., Beattie, E.C., Seo, J.Y., Malenka, R.C., 2005. Differential regulation of AMPA receptor and GABA receptor trafficking by tumor necrosis factor-alpha. J Neurosci 25, 3219-3228.

Syvanen, S., Russmann, V., Verbeek, J., Eriksson, J., Labots, M., Zellinger, C., Seeger, N., Schuit, R., Rongen, M., van Kooij, R., Windhorst, A.D., Lammertsma, A.A., de Lange, E.C., Voskuyl, R.A., Koepp, M., Potschka, H., 2013. [(11)C]quinidine and [(11)C]laniquidar PET imaging in a chronic rodent epilepsy model: Impact of epilepsy and drug-responsiveness. Nucl Med Biol 40, 764-775.

Tellez-Zenteno, J.F., Hernandez-Ronquillo, L., 2012. A review of the epidemiology of temporal lobe epilepsy. Epilepsy Res Treat 2012, 630853.

Toth, M., Little, P., Arnberg, F., Haggkvist, J., Mulder, J., Halldin, C., Gulyas, B., Holmin, S., 2016. Acute neuroinflammation in a clinically relevant focal cortical ischemic stroke model in rat: longitudinal positron emission tomography and immunofluorescent tracking. Brain Struct Funct 221, 1279-1290.

Vallez Garcia, D., de Vries, E.F., Toyohara, J., Ishiwata, K., Hatano, K., Dierckx, R.A., Doorduin, J., 2015. Evaluation of [(11)C]CB184 for imaging and quantification of TSPO overexpression in a rat model of herpes encephalitis. Eur J Nucl Med Mol Imaging 42, 1106-1118.

Van Nieuwenhuyse, B., Raedt, R., Sprengers, M., Dauwe, I., Gadeyne, S., Carrette, E., Delbeke, J., Wadman, W.J., Boon, P., Vonck, K., 2015. The systemic kainic acid rat model of temporal lobe epilepsy: Long-term EEG monitoring. Brain Res 1627, 1-11.

Vezzani, A., Aronica, E., Mazarati, A., Pittman, Q.J., 2013. Epilepsy and brain inflammation. Exp Neurol 244, 11-21.

Vezzani, A., French, J., Bartfai, T., Baram, T.Z., 2011. The role of inflammation in epilepsy. Nat Rev Neurol 7, 31-40.

Vezzani, A., Friedman, A., 2011. Brain inflammation as a biomarker in epilepsy. Biomark Med 5, 607-614.

Viviani, B., Bartesaghi, S., Gardoni, F., Vezzani, A., Behrens, M.M., Bartfai, T., Binaglia, M., Corsini, E., Di Luca, M., Galli, C.L., Marinovich, M., 2003. Interleukin-1beta enhances NMDA receptor-mediated intracellular calcium increase through activation of the Src family of kinases. J Neurosci 23, 8692-8700.

Vloeberghs, E., Van Dam, D., Franck, F., Staufenbiel, M., De Deyn, P.P., 2007. Mood and male sexual behaviour in the APP23 model of Alzheimer's disease. Behav Brain Res 180, 146-151.

Walker, A., Russmann, V., Deeg, C.A., von Toerne, C., Kleinwort, K.J., Szober, C., Rettenbeck, M.L., von Ruden, E.L., Goc, J., Ongerth, T., Boes, K., Salvamoser, J.D., Vezzani, A., Hauck, S.M., Potschka, H., 2016. Proteomic profiling of epileptogenesis in a rat model: Focus on inflammation. Brain Behav Immun 53, 138-158.

Williams, P.A., White, A.M., Clark, S., Ferraro, D.J., Swiercz, W., Staley, K.J., Dudek, F.E., 2009. Development of spontaneous recurrent seizures after kainate-induced status epilepticus. J Neurosci 29, 2103-2112.

**Highlights:**

- KASE rats display depression-like and sensorimotor-related comorbidities.
- Translocator protein PET imaging correlates severity of depression-like and sensorimotor-related comorbidities.
- Translocator protein PET imaging predicts spontaneous seizure frequency.
- Non-invasive PET imaging is a prognostic biomarker for seizure frequency and reflects severity of investigated comorbidities.

## Figures

Fig. 1. *In vivo* imaging during epileptogenesis. (A) [$^{18}$F]-PBR111 uptake 2 weeks post-SE showed high levels of TSPO binding in KASE rats ($n$ = 15) compared to control animals ($n$ = 6), not only in the limbic regions, but also in the ventricles, thalamus and hypothalamus. (**B**) [$^{18}$F]-PBR111 uptake 4 weeks post-SE demonstrated a generalized decrease in tracer uptake in KASE rats ($n$ = 15) compared to 2 weeks post-SE. However, at 4 weeks post-SE [$^{18}$F]-PBR111 binding was still higher in the thalamus, hippocampus and temporal lobe compared to control animals ($n$ = 6). (**C**) $T_2$-MRI 2 weeks post-SE showed hippocampal shrinkage in KASE animals ($n$ = 15) compared to control rats ($n$ = 6). (**D**) $T_2$-MRI 4 weeks post-SE demonstrated a significant decrease in hippocampal volume and enlargement of ventricles. Representative coronal PET and MR images are shown in **E** and **F**. Mann-Whitney U test (**A**–**D**). *$P$ < 0.05, **$P$ < 0.01, ***$P$ < 0.001. OB = olfactory bulb, FRONT = frontal cortex, INS = insular cortex, PIR = anterior piriform cortex, THAL = thalamus, HYP = hypothalamus, HC = hippocampus, TEMP = extrahippocampal temporal lobe, CB = cerebellum, WB = whole brain, KASE = kainic acid-induced status epilepticus.

Fig. 2. Comorbidities during chronic epilepsy are reflected by [$^{18}$F]-PBR111 uptake during epileptogenesis. (A) Whisker nuisance response 9 weeks after SE, KASE animals ($n$ = 11) displayed significantly increased behavioral response in comparison with controls ($n$ = 3). [$^{18}$F]-PBR111 uptake in the hippocampus 2 and 4 weeks post-SE correlated with whisker nuisance scores 9 weeks post-SE (**B**-**C**). Whisker nuisance response 11 weeks after SE, KASE animals ($n$ = 11) displayed significantly increased behavioral response in comparison with controls ($n$ = 3) (**D**). [$^{18}$F]-PBR111 uptake in the hippocampus 2 and 4 weeks post-SE correlated with whisker nuisance scores 11 weeks post-SE (**E**-**F**). (**G**) Sucrose consumption 12 weeks post-SE. KASE rats ($n$ = 11) showed reduced sucrose consumption compared to control animals ($n$ = 3). Negative significant correlations could be determined between [$^{18}$F]-PBR111 uptake in the hippocampus 2 and 4 weeks post-SE and sucrose preference 12 weeks post-SE (**H**-**I**). (**J**) Immobility time during FST 12 weeks post-SE. KASE rats ($n$ = 15) spent a longer period of time immobile compared to controls ($n$ = 6). The time spent immobile during the FST significantly correlated with [$^{18}$F]-PBR111 uptake in hippocampus 2 and 4 weeks post-SE (**K**-**L**). Open circles represent control animals; full circles represent KASE rats (**B**-**C**, **E**-**F**, **H**-**I**, and **K**-**L**). Two-way repeated measures ANOVA (**A**, **D**). Mann-Whitney U test (**G**, **J**). Pearson correlation (**B**-**C**, **E**-**F**, **H**-**I**, and **K**-**L**). *$P$ < 0.05, **$P$ < 0.01. SE = status epilepticus, HC = hippocampus, WNT = Whisker nuisance task, SPT = sucrose preference test, FST = forced swim test, KASE = kainic acid-induced status epilepticus. Correlations of the other brain regions investigated are reported in Table 1.

Fig. 3. [$^{18}$F]-PBR111 PET 2 weeks post-SE predicts SRS outcome. (A) Principal component analysis (PCA) of [$^{18}$F]-PBR111 2 weeks post-SE ($n$ = 21). PCA represents PET data in a two-dimensional space accounting for 80% of the total variability of the dataset. (**B**) Contribution of

each VOI to explaining PCA variability. VOIs above the red line had a major influence; the temporal lobe and hippocampus were found to be the most relevant regions in explaining the variability in the dataset. (**C**) Differences in SRS experienced by the three subcategories of KASE animals determined based on PCA. Absent or rare SRS ($n$ = 4), sporadic SRS ($n$ = 7) and frequent SRS ($n$ = 4). A Kruskal-Wallis test with a post-hoc Dunn's multiple comparison test. $^{**}P < 0.01$. (**D**) Partial least squares regression generated a model that can predict SRS frequency for each subject ($n$ = 15). The graph reports the number of experienced SRS/day (measured) versus the number of predicted SRS/day (estimated) for the model. Spearman's rank correlation. Each symbol represents one animal (**A**, **C** and **D**). SRS = spontaneous recurrent seizures; OB = olfactory bub, FRONT = frontal cortex, IC = insular cortex, PIR = anterior piriform cortex, THA = thalamus, HYP = hypothalamus, HC = hippocampus, TEMP = extrahippocampal temporal lobe, CB = cerebellum.

Table 1. Correlation between [$^{18}$F]-PBR111 PET imaging during epileptogenesis and comorbidities during chronic epilepsy (9-12 weeks post-SE). R = Pearson correlation coefficient, $R^2$ = Coefficient of determination. $^{*}P < 0.05$, $^{**}P < 0.01$, $^{***}P < 0.001$, $^{****}P < 0.0001$. Statistically significant correlations are indicated in bold. SE = status epilepticus, VOI = Volume of interest.

| **Measure** | **VOI** | **[$^{18}$F]-PBR111 PET SUV 2w post-SE** | | | | **[$^{18}$F]-PBR111 PET SUV 4w post-SE** | | | |
|---|---|---|---|---|---|---|---|---|---|
| | | **R** | ***P*-value** | **$R^2$** | ***F*** | **R** | ***P*-value** | **$R^2$** | ***F*** |
| Whisker nuisance task 9w post-SE | Olfactory Bulb | 0.35 | 0.2108 | 0.12 | 1.68 | 0.47 | 0.2217 | 0.22 | 3.51 |
| | Frontal Cortex | 0.32 | 0.2583 | 0.10 | 1.42 | 0.49 | 0.2337 | 0.24 | 3.79 |
| | Insular Cortex | **0.67**** | **0.0079** | **0.45** | **10.02** | **0.68**** | **0.0068** | **0.47** | **10.78** |
| | Piriform Cortex | **0.59*** | **0.0236** | **0.35** | **6.59** | **0.58*** | **0.0303** | **0.34** | **6.19** |
| | Ventricles | **0.78***** | **0.0009** | **0.61** | **18.88** | **0.79***** | **0.0007** | **0.63** | **20.90** |
| | Thalamus | 0.45 | 0.1007 | 0.20 | 3.18 | 0.51 | 0.0614 | 0.2 | 4.33 |

| | | | | | | | | | |
|---|---|---|---|---|---|---|---|---|---|
| | | | | | 6 | | | | |
| | Hypothalamus | **0.73**** | **0.0030** | **0.53** | **13.75** | **0.75**** | **0.0020** | **0.56** | **15.84** |
| | Hippocampus | **0.87***** | **<0.0001** | **0.75** | **36.99** | **0.67**** | **0.0084** | **0.50** | **12.23** |
| | Temporal Lobe | **0.77**** | **0.0012** | **0.59** | **17.56** | **0.77**** | **0.0025** | **0.59** | **17.57** |
| | Cerebellum | 0.29 | 0.3017 | 0.08 | 1.13 | 0.49 | 0.0744 | 0.24 | 3.92 |
| Whisker nuisance task 11w post-SE | Olfactory Bulb | **0.55*** | **0.0377** | **0.31** | **5.45** | **0.58*** | **0.0267** | **0.32** | **5.68** |
| | Frontal Cortex | 0.38 | 0.1007 | 0.33 | 2.12 | **0.56*** | **0.0372** | **0.31** | **4.82** |
| | Insular Cortex | **0.62*** | **0.0158** | **0.39** | **7.88** | **0.63*** | **0.0152** | **0.28** | **4.81** |
| | Piriform Cortex | **0.68**** | **0.0069** | **0.46** | **10.59** | **0.59*** | **0.0247** | **0.32** | **5.72** |
| | Ventricles | **0.79***** | **0.0007** | **0.63** | **20.67** | **0.77**** | **0.0013** | **0.59** | **17.53** |
| | Thalamus | **0.61*** | **0.0203** | **0.37** | **7.14** | **0.62*** | **0.0176** | **0.38** | **7.57** |
| | Hypothalamus | **0.77**** | **0.0011** | **0.60** | **18.26** | **0.72**** | **0.0029** | **0.52** | **13.47** |
| | Hippocampus | **0.76**** | **0.0013** | **0.60** | **18.66** | **0.73**** | **0.0025** | **0.57** | **16.15** |
| | Temporal Lobe | **0.61*** | **0.0261** | **0.37** | **6.59** | **0.59*** | **0.0324** | **0.35** | **5.98** |
| | Cerebellum | 0.30 | 0.2365 | 0.09 | 1.24 | **0.53*** | **0.0492** | **0.28** | **3.74** |
| Sucrose preference test 12w post-SE | Olfactory Bulb | -0.21 | 0.4716 | 0.04 | 0.55 | **-0.58*** | **0.0286** | **0.42** | **7.29** |
| | Frontal Cortex | -0.23 | 0.4470 | 0.05 | 0.62 | -0.57 | 0.0530 | 0.33 | 4.95 |
| | Insular Cortex | **-0.60*** | **0.0294** | **0.36** | **6.26** | **-0.69*** | **0.0149** | **0.48** | **9.46** |
| | Piriform Cortex | -0.52 | 0.0664 | 0.27 | 4.15 | **-0.63*** | **0.0404** | **0.39** | **6.66** |
| | Ventricles | **-0.60*** | **0.0278** | **0.36** | **6.41** | **-0.63*** | **0.0159** | **0.40** | **7.33** |
| | Thalamus | -0.43 | 0.1394 | 0.18 | 2.53 | -0.49 | 0.0709 | 0.24 | 3.60 |
| | Hypothalamus | -0.41 | 0.1586 | 0.17 | 2.28 | **-0.60*** | **0.0206** | **0.48** | **9.37** |
| | Hippocampus | **-0.76**** | **0.0013** | **0.58** | **15.47** | **-0.81***** | **0.0004** | **0.69** | **22.76** |
| | Temporal Lobe | **-0.80***** | **0.0010** | **0.64** | **19.95** | **-0.84***** | **0.0008** | **0.71** | **25.18** |
| | Cerebellum | -0.13 | 0.6539 | 0.01 | 0.21 | -0.46 | 0.1675 | 0.21 | 2.68 |
| Forced swim test 12w post-SE | Olfactory Bulb | -0.14 | 0.5205 | 0.025 | 0.42 | **0.47*** | **0.0287** | **0.22** | **5.06** |
| | Frontal Cortex | -0.19 | 0.3910 | 0.038 | 0.77 | **0.52*** | **0.0155** | **0.27** | **7.07** |
| | Insular Cortex | 0.42 | 0.0524 | 0.18 | 4.28 | **0.68***** | **0.0005** | **0.47** | **17.25** |
| | Piriform Cortex | 0.22 | 0.3375 | 0.05 | 0.96 | **0.65**** | **0.0014** | **0.42** | **13.96** |
| | Ventricles | **0.56**** | **0.0072** | **0.32** | **9.06** | **0.63**** | **0.0020** | **0.40** | **12.74** |
| | Thalamus | 0.25 | 0.2618 | 0.06 | 1.33 | **0.61**** | **0.0030** | **0.3** | **11.5** |

| | | | | | | | | |
|---|---|---|---|---|---|---|---|---|
| | | | | | | | **7** | **6** |
| Hypothalamus | 0.31 | 0.1644 | 0.09 | 2.09 | 0.28 | 0.2084 | 0.08 | 1.96 |
| Hippocampus | **0.54*** | **0.0110** | **0.29** | **7.94** | **0.63**** | **0.0019** | **0.40** | **12.98** |
| Temporal Lobe | **0.66**** | **0.0011** | **0.43** | **14.86** | **0.69***** | **0.0005** | **0.47** | **17.45** |
| Cerebellum | 0.22 | 0.3278 | 0.05 | 1.01 | **0.55**** | **0.0084** | **0.31** | **8.63** |

Fig 1

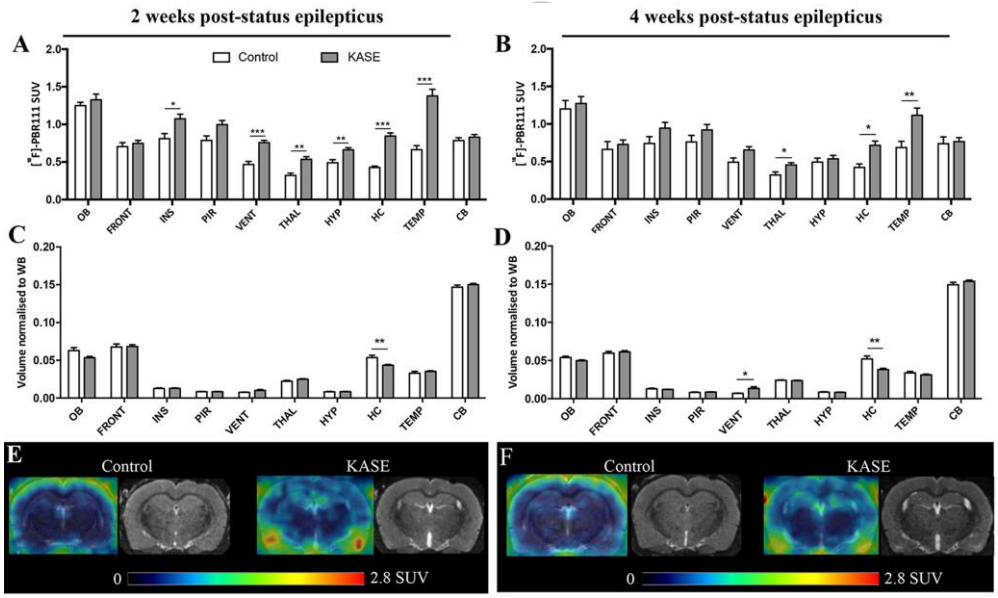

Fig.2

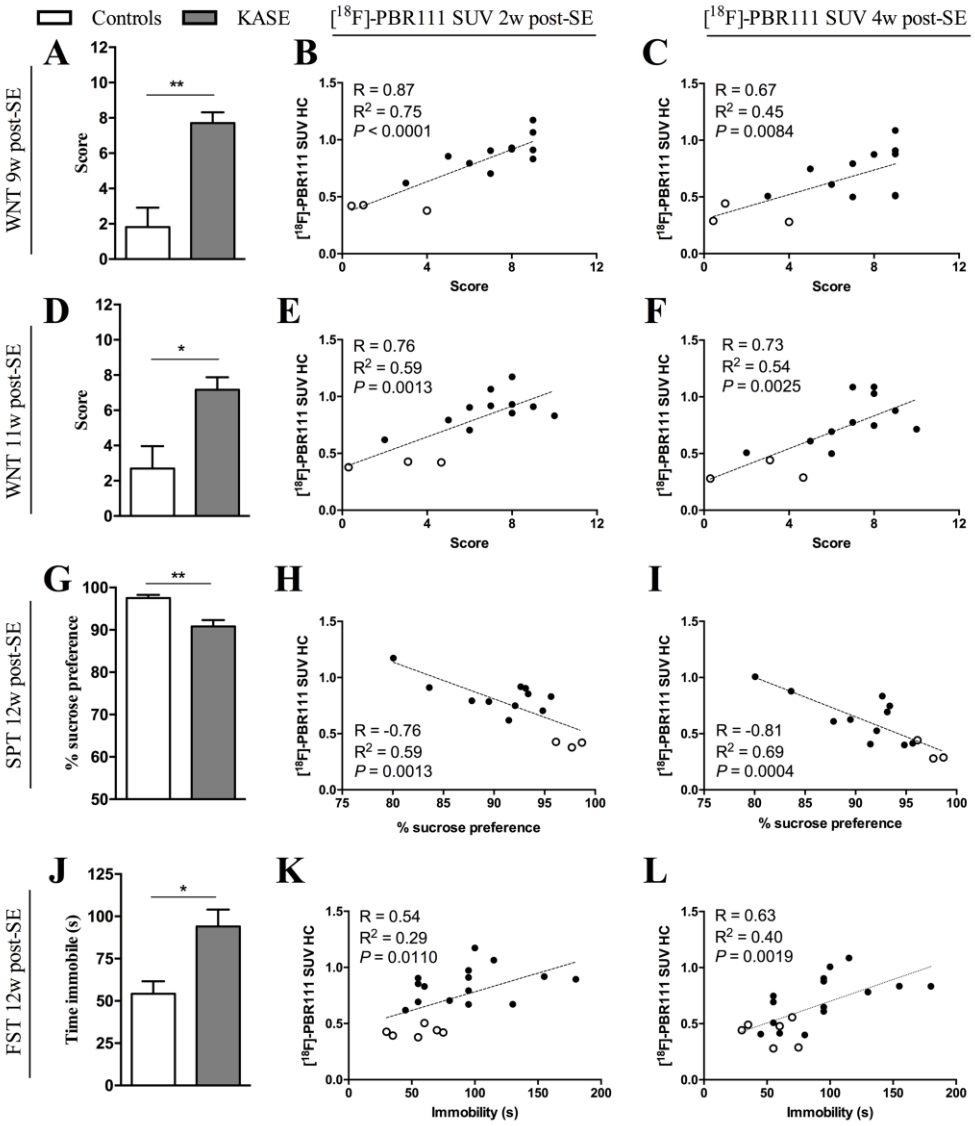

Fig 3